

Ultra-broadband acoustic logic gate based on passive phase manipulation

Yu-Han Xia(夏宇涵), Nai-Qi Pang(庞乃琦), Yin Wang(王垠), Long-Xu Wang(王龙旭), and Yong Ge(葛勇)
Citation: Chin. Phys. B, 2026, 35 (**1**): 014301. DOI: 10.1088/1674-1056/ade667
http://cpb.iphy.ac.cn; http://iopscience.iop.org/cpb

What follows is a list of articles you may be interested in

Effect of metal plate on ultrasonic cavitation field distribution

Jin-He Liu(刘金河), Zhuang-Zhi Shen(沈壮志), Peng-Fei Cao(曹鹏飞), Jian-Feng Li(李建锋), and Xiao-Qiang Bai(白小强)
Chin. Phys. B, 2025, 34 (**5**): 054302. DOI: 10.1088/1674-1056/adca9d

Acoustic wave propagation in a porous medium saturated with two fluids and a solid

Lin Liu(刘琳), Xiu-Mei Zhang(张秀梅), and Xiu-Ming Wang(王秀明)
Chin. Phys. B, 2025, 34 (**2**): 024301. DOI: 10.1088/1674-1056/ad9d17

Orbital angular momentum conversion of acoustic vortex beams via planar lattice coupling

Qingbang Han(韩庆邦), Zhipeng Liu(刘志鹏), Cheng Yin(殷澄), Simeng Wu(吴思梦), Yinlong Luo(罗寅龙), Zixin Yang(杨子鑫), Xiuyang Pang(庞修洋), Yiqiu Wang(王溢秋), Xuefen Kan(阚雪芬), Yuqiu Zhang(张雨秋), Qiang Yu(俞强), and Jian Wu(吴坚)
Chin. Phys. B, 2024, 33 (**9**): 094301. DOI: 10.1088/1674-1056/ad57ad

Pipeline thickness estimation using the dispersion of higher-order SH guided waves

Zhengchen Dai(代政辰), Jinxia Liu(刘金霞), Yunfei Long(龙云飞), Jianhai Zhang(张建海), Tribikram Kundu, and Zhiwen Cui(崔志文)
Chin. Phys. B, 2024, 33 (**7**): 074301. DOI: 10.1088/1674-1056/ad3033

Experimental realization of fractal fretwork metasurface for sound anomalous modulation

Jiajie He(何佳杰), Shumeng Yu(于书萌), Xue Jiang(江雪), and Dean Ta(他得安)
Chin. Phys. B, 2024, 33 (**5**): 054301. DOI: 10.1088/1674-1056/ad2dcd

---

Ultra-broadband acoustic logic gate based on passive phase manipulation

Yu-Han Xia(夏宇涵)[1,†], Nai-Qi Pang(庞乃琦)[1,†], Yin Wang(王垠)[1], Long-Xu Wang(王龙旭)[2], and Yong Ge(葛勇)[1,2,‡]

[1] *School of Physics and Electronic Engineering, Jiangsu University, Zhenjiang* 212013, *China*
[2] *State Key Laboratory of Acoustics and Marine Information, Institute of Acoustics, Chinese Academy of Sciences, Beijing* 100190, *China*

(Received 1 April 2025; revised manuscript received 29 May 2025; accepted manuscript online 20 June 2025)

In recent years, acoustic logic gates has attracted growing interest in acoustics due to their promising applications in acoustic communication and signal processing. For practical implementation, these logic gates must operate over a certain bandwidth to ensure reliable performance. However, current experimental realizations have predominantly been confined to single-frequency or narrowband operation, leaving their broadband capabilities largely unverified. To address this gap, we present both numerical and experimental demonstrations of three basic acoustic logic gates (OR, NOT, and AND) using a phased unit cell composed of a central channel flanked by two arrays of semicircular cavities. By leveraging phase modulation of the unit cells and linear interference of sound, we achieve these logic operations with a uniform threshold of $I_t = 0.25$. Remarkably, the measured fractional bandwidths (bandwidth relative to center frequency) reach approximately 111.5% (OR), 37.2% (NOT), and 48.5% (AND), demonstrating ultra-broadband functionality. The proposed logic gates combine exceptional bandwidth with structural simplicity, offering significant potential for applications in acoustic computing, information processing, and integrated acoustic systems.

Keywords: acoustic logic gate, ultra-broad band, phased unit cell

PACS: 43.20.+g, 43.60.+d

DOI: 10.1088/1674-1056/ade667 **CSTR:** 32038.14.CPB.ade667

1. Introduction

As the cornerstone of digital circuit technology, logic gate has attracted increasing attentions from researchers due to its significant potential applications in various scenarios, such as the chips for intelligent agricultural machinery,[1,2] food treatment,[3,4] information processing,[5,6] and optical communications.[7,8] Motivated by the possibilities of novel advanced devices, this concept is introduced into the other fields.[9,10] Especially in the field of optics, various optical logic gates with high-efficiency have been demonstrated both theoretically and experimentally.[11–17]

Inspired by the optical logic gate, an analogous concept has also been proposed in acoustics. With the rapid development of sonic crystals[18–22] and acoustic metamaterials,[23–33] the design of acoustic logic gates (ALGs) has become a research hotspot due to its various important potential applications in computing, information processing, and integrated acoustics. Based on the nonlinear dynamical effect, the logic functions AND and OR have been experimentally realized in a driven granular chain composed of spherical particles.[34] By introducing the linear interference mechanisms of sound, several ALGs have been realized theoretically and experimentally based on the sonic crystals.[35,36] Furthermore, by employing density-near-zero metamaterials, a series of ALGs and corresponding logic operations have also been demonstrated[37] with the active manipulations of the phases of input and control signals. In addition, by attaching acoustic metasurfaces to the inner walls of straight[38] or curved[39] waveguides, basic logic gates have also been realized with the phases of the input sounds modulated by passive structures. Recently, the acoustic topological insulators[40–43] with the backscattering immunity characteristics have been introduced to design various robust acoustic devices with tunable or multiple logic functionalities.[44–47] Although these previous works have realized ALGs with high-efficiency, their working bandwidth is limited due to the local resonance of acoustic metamaterials. However, for practical implementation, the logic gate must operate over a broad bandwidth to ensure reliable performance.

To overcome this problem, a multi-port circular waveguide-based ALG with a working bandwidth exceeding 5 kHz has been proposed,[48] in which the phases of input and control signals are actively manipulated. However, the experimental verification of logical functions with ultra-broad band is seldom reported. Therefore, it is still a significant challenge to experimentally realize ALGs with ultra-broad bandwidth and passive structure simultaneously.

[†]These authors contributed equally to this work.
[‡]Corresponding author. E-mail: geyong@ujs.edu.cn

© 2026 Chinese Physical Society and IOP Publishing Ltd. All rights, including for text and data mining, AI training, and similar technologies, are reserved.

In this work, we propose an ultra-broadband ALG utilizing a type of phased unit cell, which consists of a central channel and two arrays semicircular cavities on both sides. Based on the phase manipulation of the phased unit cells and the linear interference of sound, we both numerically and experimentally design and demonstrate the performance of three basic ALGs (OR, NOT, and AND) with the uniform threshold 0.25. In addition, we measure the working bandwidth of the logic gates OR, NOT, and AND, and their fractional bandwidths (the ratio of the bandwidth to the center frequency) are approximately 111.5%, 37.2%, and 48.5%, respectively. Following the introduction, Section 2 delineates the characteristics of the phased unit cells. Section 3 elaborates on the theory of linear interference of sound. The designs and performance evaluations of the ALGs OR, NOT, and AND are detailed in Sections 4, 5, and 6, respectively. Section 7 investigates the bandwidths of these three basic ALGs, encompassing the measurement methods and models. Experimental validations are presented throughout Sections 3–7 to substantiate the simulated findings. Finally, Section 8 concludes the study by summarizing the key contributions and insights of this work.

2. Design of phased unit cells

In this section, we present the design of the phased unit cells, along with their transmission properties, phase delay characteristics, and the phase-difference spectra. To realize a broadband ALG, as schematically shown in Fig. 1(a), we design a type of phased unit cell with the height of H composed of a central channel and two arrays of five semicircular cavities on both sides. Figure 1(b) shows the cross-section of the phased unit cell. The width w and the length l are selected as 1 cm and 5 cm, respectively, the height of the central channel h can be tailored to manipulate the transmitted phase delay of sound, and the radius r of each semicircular cavity is determined by $r = (w-h)/2$. The incident wavelength λ is selected as 5 cm (viz., the frequency $f = 6.86$ kHz in air). The phased unit cell is fabricated with epoxy resin based on the three-dimensional (3D) printing technology. Throughout this work, we use the COMSOL Multiphysics software to simulate the propagation characteristics of sound. In the models, the boundaries of both input and output ports are selected as the plane wave radiation, the other ones are set as the hard sound boundary, and the material parameters of air are selected as $\rho = 1.21$ kg/m^3 and $c = 343$ m/s.

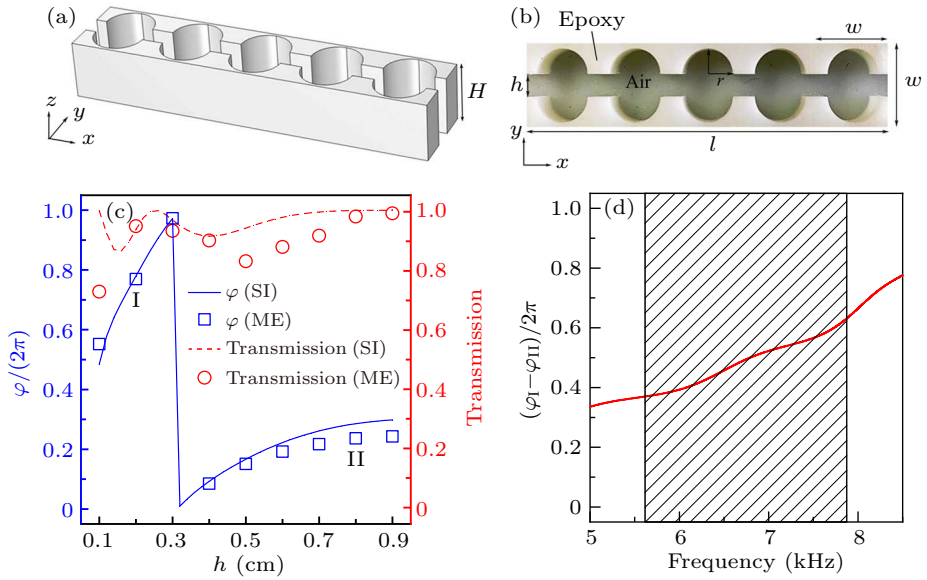


Fig. 1. (a) Schematic diagram of a phased unit cell and (b) its cross-section. (c) Measured (ME) and simulated (SI) transmission coefficients and phase delays caused by the phased unit cells with different values of h at 6.86 kHz. (d) Simulated phase-difference spectrum of phased unit cells I and II.

To demonstrate the performance of the phased unit cells with different values of h, we conduct an experiment to measure the transmission coefficients and phase delays of sound. The details of the experimental set-up are exhibited in note 1 of the supplementary material. Figure 1(c) shows the measured transmission coefficients (red open circles) and phase delays (blue open squares) caused by the phased unit cells with different values of h, and the corresponding simulated ones (red dashed and blue solid lines) are also plotted for comparison. We observe that, in the range 0.1 cm–0.9 cm, the phase delay of sound can covers the whole range of 2π, and most transmission coefficients are larger than 0.7. The measured results basically agree with the simulated ones. To design ALGs OR and NOT, we here select two phased unit cells with $h = 0.2$ cm and 0.8 cm (denoted as I and II), which correspond to the simulated transmission coefficients of 0.95 and 0.98 and the difference of the phase delays $\varphi_{\rm I} - \varphi_{\rm II}$ nearly equals π. The simulated pressure distributions caused by the phased unit cells I

and II are shown in note 2 of the supplementary material, in which the transmitted acoustic pressure profiles caused by the the phased unit cells I and II are quite strong and obviously exhibit opposite phase delays. In addition, we simulate the phase-difference spectrum of the phased unit cells I and II, as shown in Fig. 1(d). The phase-difference ranges from 0.76π to 1.24π, which approximately centered around π within the frequency range of 5.62 kHz–7.87 kHz (indicated by the black shaded region). Furthermore, the transmission spectra of the phased unit cells I and II are provided in note 2 of the supplementary material. The results show that the phased unit cells I and II keep high transmission in the frequency ranges 4 kHz–9 kHz and 4 kHz–14 kHz, respectively. Leveraging these broadband characteristics, we can design ALGs with ultra-broadband performance.

3. Theory of linear interference of sound

In this section, we provide a concise introduction to the theory of linear sound interference, which serves as one of the fundamental principles underlying the designed ALGs. Typically, the pressures of two sound waves, A and B, can be expressed as

$$p_{\mathrm{A}} = A_1 \cos\left(2\pi f t + \varphi_{\mathrm{A}} - \frac{2\pi f}{c} s\right), \tag{1}$$

$$p_{\mathrm{B}} = A_2 \cos\left(2\pi f t + \varphi_{\mathrm{B}} - \frac{2\pi f}{c} s\right), \tag{2}$$

where f is the frequency, t represents the time, c denotes the sound speed, φ_{A} and φ_{B} are the initial phases, A_1 and A_2 are amplitudes, and s is the propagation distance of the sound. When these two sound waves converge at a specific point O, their pressures superimpose according to the principle of linear superposition, described by

$$p_{\mathrm{O}} = p_{\mathrm{A}} + p_{\mathrm{B}}. \tag{3}$$

The resultant amplitude A is determined by

$$A = \sqrt{A_1^2 + A_2^2 + 2A_1A_2\cos(\Delta\varphi)}, \tag{4}$$

and the phase difference $\Delta\varphi$ is given by

$$\Delta\varphi = \varphi_{\mathrm{B}} - \varphi_{\mathrm{A}} - \frac{2\pi f}{c}(s_{\mathrm{A}} - s_{\mathrm{B}}), \tag{5}$$

where s_{A} and s_{B} represent the propagation distances of sound waves A and B, respectively. When the phase difference is an even multiple of π, the resultant amplitude A reaches its maximum value ($A = A_1 + A_2$), indicating constructive interference between the two sound waves. Conversely, when the phase difference is an odd multiple of π, A is minimum ($A = |A_1 - A_2|$), signifying the interference cancellation of two sounds.

4. Design and performances of ALG OR

Herein, we detail the design of ALG OR and demonstrate its working principles along with performance. Figure 2(a) schematically shows the designed ALG OR composed of a circular waveguide with the inner radius of r_1 and the outer radius of r_2 and three straight waveguides (A, B, and O) with the width of w. Two phased unit cells II are attached on the inner surface of the waveguides A and B. The waveguides A and B are the two input ports, and the waveguide O is the output port for the logic gate OR, and the incident sound signals from the input ports A and B have the same initial phase and amplitude. Thus, when the sound signals are incident from both input ports A and B simultaneously, the interference enhancement exists at the port O owing to the same phased unit cells in the input ports A and B, and the output pressure amplitude is determined by Eqs. (4) and (5). Moreover, when the sound signal is separately incident from the input ports A or B, the sound energy at the output port O is still strong due to the high transmission of the phased unit cell II, providing the feasibility of realizing the logic function OR. The detail of the principle of ALG OR is presented in note 3 of the supplementary material. The sample photograph of the logic gate OR is shown in Fig. 2(b).

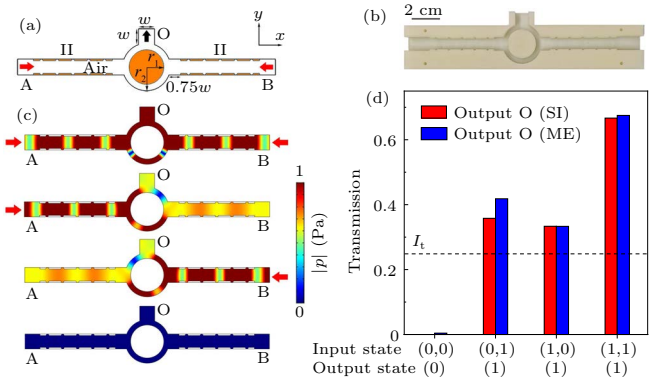


Fig. 2. (a) Schematic diagram of an ALG OR, and (b) its sample photograph. (c) Simulated pressure amplitude distributions through the logic gate OR with different input states at 6.86 kHz. (d) Measured (ME) and simulated (SI) transmission coefficients for different input states. The red arrows in panels (a) and (c) represent input sound signals and the black arrow in panel (a) refers to output sound signals.

To exhibit the performances of the logic gate OR, we simulate the pressure amplitude distributions through the logic gate for different input states at 6.86 kHz. Here, we define the input state of the logic gate as (Q_1, Q_2), in which Q_i represents whether there exist sound signals emitted from the input ports A and B or not, denoting as Q_i ="1" or "0", respectively. In addition, to evaluate the output states of the logic gate, we select a uniform threshold $I_{\mathrm{t}} = 0.25$. When the transmission coefficient is larger than I_{t}, the output state is (1), otherwise is (0). As shown in Fig. 2(c), for the input states (1,1), (1,0), and (0,1), the pressure amplitudes around the output port O are very large, in which the output amplitude for the input state

(1,1) is about two times than those for the input states (1,0) and (0,1). However, for the input state (0,0), the pressure amplitude at the output port O is zero. To experimentally demonstrate it, we measure the transmission coefficients of the logic gate OR for different input states at 6.86 kHz, and the simulated results are also provided for comparison. As shown in Fig. 2(d), based on the uniform threshold $I_t = 0.25$, the output states are (0), (1), (1), and (1) for the input states (0,0), (0,1), (1,0), and (1,1), showing high performance of the logic gate OR. The measured and simulated results are consistent with each other.

5. Design and performances of ALG NOT

In this section, we present the design of ALG NOT, and demonstrate its performance and working principle. By replacing the phased unit cell II in the waveguide A with the phased unit cell I, we can design a type of ALG NOT, in which the other structure parameters are the same as those of the ALG OR in Fig. 2(a). As shown in Fig. 3(a), the waveguide B is set as the control port with a constant input sound signal, and the waveguides A and O are the input and output ports, respectively. In addition, similar to the logic gate OR, the input sound sources at the input and control ports are the same. The sample photograph of the logic gate NOT is presented in Fig. 3(b).

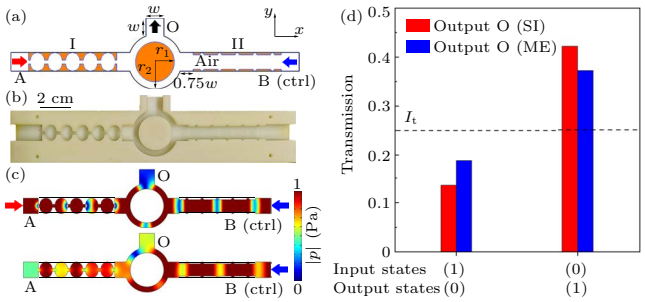


Fig. 3. (a) Schematic diagram of an ALG NOT, and (b) its sample photograph. (c) Simulated pressure amplitude distributions through the logic gate NOT with different input states at 6.86 kHz. (d) Measured and simulated transmission coefficients for different input states. The red and blue arrows in panels (a) and (c) represent the input and control sound signals, respectively, and the black arrow in panel (a) is the output sound signal.

As shown in Fig. 1(c), the phase difference between phased unit cells I and II is π, and thus the transmitted sound signals through the phased unit cells at the ports A and B are out of phase, leading to the interference cancellation of sound at the output port O. However, when there is no input sound signal from the port A, the sound energy from the control port B can still reach the output port O with high transmission. The detail of the principle of ALG NOT is presented in note 4 of the supplementary material. To further demonstrate the performance of the ALG NOT, we simulate the pressure amplitude distributions through the logic gate NOT for different input states at 6.86 kHz. As shown in Fig. 3(c), the pressure amplitude at the output port O is almost zero for the input state (1), which is attributed to the interference cancellation owing to the phase manipulation of sound caused by the phased unit cells I and II. However, for the input state (0), the output sound energy is clearly observed at the output port O. To experimentally demonstrate the logic function NOT, we measure and simulate the transmission through the logic gate NOT for different input states at 6.86 kHz, and the simulated results are also presented for comparison in Fig. 3(d). We observe that both the measured and simulated transmission coefficients for the input state (0) are higher than I_t, whereas those for the input state (1) are lower than I_t, showing high performance of the designed logic gate NOT.

6. Design and performance of ALG AND

In this section, we introduce the design of ALG AND, and elucidate its principle and performance. Figure 4(a) schematically shows the designed ALG AND composed of a circular waveguide and four connected straight waveguides (A, B, C, and O). The structural parameters are the same as those in Fig. 2(a). The waveguides A and B are the two input ports, and the waveguides C and O are the control port with a constant sound signal and the output port for the ALG AND, respectively. To realize the ALG AND, in addition to the phased unit cells I attached to the inner surfaces of the input ports A and B, we here introduce another type of phased unit cell into the waveguide C as the control port, in which a rectangular solid is added at its lower-left end to reduce the transmission coefficient of the input sound signal. The phase delays and transmission coefficients of the phased unit cells with different values of h are presented in note 5 of the supplementary materials. Here, we select the phased unit cell III with the transmission coefficient of 0.7 and the same phase delay as that of the phased unit cell I, which is used to realize the transmission of the ALG AND less than 0.25 for the input state (0,0) and the interference cancellation between the input and control signals around the output port O. The sample photograph of the ALG AND is shown in Fig. 4(b).

Figure 4(c) shows the simulated pressure amplitude distributions through the ALG AND for different input states at 6.86 kHz. We can see that the output pressure amplitude at the output port O is very large for the input state (1,1), though slightly weaker than that of the ALG OR [Fig. 2(c)] due to partial interference cancellation caused by the sound signal from the control port C. In addition, for the input states (1,0) and (0,1), the output pressure amplitudes are significantly suppressed due to the interference cancellation caused by the sound signals from the ports A and C and the ports B and C,

respectively. Finally, for the input state (0,0), the pressure amplitude at the output port O is small, but is still observed. Such a phenomenon arises from the relatively small transmission coefficient of the phased unit cell III and the sound energy transmitted through port C is dispersed into the three ports A, B, and O. The details of the principles of the ALG AND for different input states are presented in note 6 of the supplementary material.

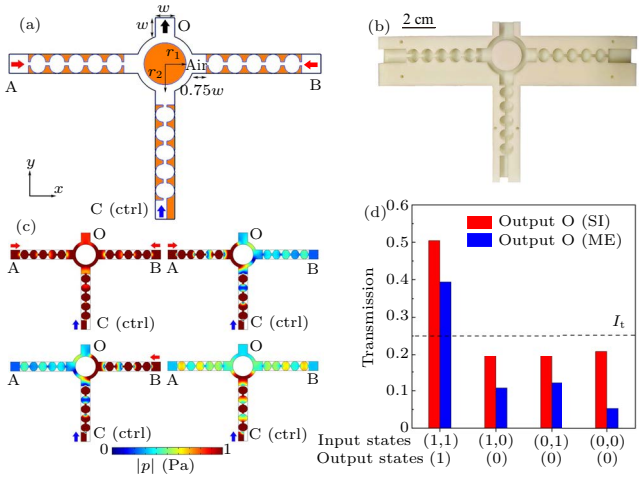


Fig. 4. (a) Schematic diagram of an ALG AND, and (b) its sample photograph. (c) Simulated pressure amplitude distributions through the ALG AND with different input states at 6.86 kHz. (d) Measured and simulated intensity levels at the output port O for different input states. The red and blue arrows in panels (a) and (c) represent the input and control sound signals, respectively, and the black arrow in panel (a) refers to the output sound signal.

To demonstrate the performance of the ALG AND, we experimentally measure the transmission through the ALG for different input states at 6.86 kHz, with simulated results plotted for comparison. As shown in Fig. 4(d), by using the uniform threshold $I_t = 0.25$, the measured output states are (1), (0), (0), and (0) for the input states (1,1), (1,0), (0,1), and (0,0), respectively, showing typical characteristics of the logic function AND. The measured results are still consistent with the simulations.

7. Bandwidth of ALGs OR, NOT and AND

In this section, we present both experimental and numerical investigations of the broadband characteristics for the acoustic logic gates (ALGs) OR, NOT, and AND, along with the corresponding method for measuring their transmission spectra under different input states. Figures 5(a)–5(c) illustrate the measurement setups for the transmission spectra of the OR, NOT, and AND gates, respectively. For ALG OR, as shown in Fig. 5(a), a pair of sound sources (red stars) with identical initial phases are positioned at input ports A and B to excite the input signals. A microphone (Mic.) placed at output port O records the sound amplitude across frequencies. To account for the source characteristics, we measure the frequency response of a single sound source in a straight waveguide of the same length as port A, and the relative amplitude spectra of the ALG OR are derived by normalizing the output amplitude against the frequency response. For transmission spectra, the maximum relative amplitude of the input state (1,0) serves as the reference signal, and the final spectra are obtained by further normalizing the relative amplitudes to this reference. The same measurement method for the ALGs NOT and AND is applied, in which the identical reference signal is adopted for consistency. In addition, the simulation models for the OR, NOT, and AND gates are the same as the configurations in Figs. 2(a), 3(a), and 4(a), respectively. Plane wave radiation conditions are applied at the boundaries between the ports (A, B, C, and O) and the external domain. The simulated transmission spectra are computed by normalizing the output amplitude spectra to the same reference signal as in experiments.

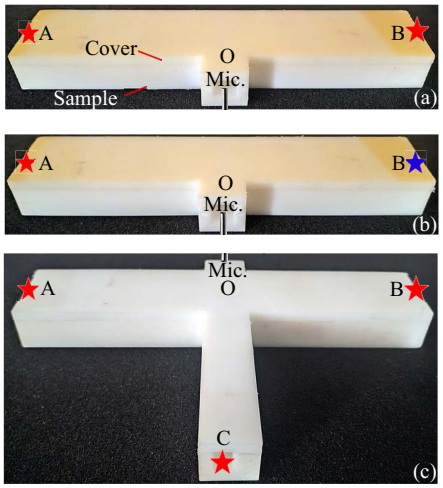


Fig. 5. Models for the measurement of the transmission spectra of the ALGs (a) OR, (b) NOT, and (c) AND, respectively. Red stars in panels (a) and (c) represent the sound sources with the same initial phases, and a blue and red stars in panel (b) represent the ones with opposite initial phases.

The designed ALGs exhibit broadband characteristics. To experimentally validate this, we measure the transmission spectra of the ALGs OR, NOT, and AND for different input states, with the simulated results also presented for comparison. As shown in Fig. 6(a), for the ALG OR, the measured transmission coefficients for the input states (1,1), (1,0), and (0,1) are higher than $I_t = 0.25$, while those for the input state (0,0) are nearly zero within the frequency range 4.66 kHz–12.31 kHz (the black shaded region). Consequently, the measured fractional bandwidth reaches approximately 111.5%, demonstrating the ultra-broadband characteristic of the ALG OR. However, a distinct transmission peak (exceeding 1.6) is observed at 5.74 kHz in Fig. 6(a), likely attributed to unintended reflections within the sample of ALG OR. As illustrated in Fig. 5(a), the cross-sectional area of port O in the ALG OR is limited to 1 cm×1 cm. When sound waves propagate from port O into the external free space, a significant

impedance mismatch at the interface can induce strong reflections. Consequently, for the input state (1,1), the output sound amplitude is markedly amplified due to the combined effects of reflection and constructive interference, resulting in a pronounced transmission peak within the working band of the ALG OR. Figure 6(b) shows the simulated transmission spectra of the ALG OR, with a working band ranging from 5.20 kHz to 12.70 kHz (black shaded region) and a fractional bandwidth of approximately 109.3%, which closely matches the measured results in Fig. 6(a). This ultra-broad bandwidth arises from the interference enhancement of sound signals through two phased unit cells II. For the ALG NOT, the measured working band [the black shaded regions in Fig. 6(c)] is in the range 5.62 kHz–8.17 kHz, with a fractional bandwidth of about 37.2%, roughly one-third that of ALG OR in Fig. 6(a). This result is primarily attributed to the difference in initial phases of sound signals passing through phased unit cells I and II. The simulated working band of the ALG NOT [the black shaded regions in Fig. 6(d)] is slightly narrower than the measured one in Fig. 6(c). Additionally, as depicted in Fig. 6(e), the measured working band (black shaded region) of the ALG AND ranges from 5.44 kHz to 8.77 kHz, with a fractional bandwidth of approximately 48.5%. In contrast, the simulated working band [black shaded region in Fig. 6(f)] of the ALG AND extends from 5.44 kHz to 9.19 kHz, with a fractional bandwidth of about 54.7%, which is slightly larger than the measured value in Fig. 6(e). Overall, the measured and simulated working bands of these designed ALGs are basically consistent with each other. Therefore, we have both numerically and experimentally demonstrated the ultra-broad bandwidths of the designed ALGs OR, NOT, and AND, in which the measured fractional bandwidths are 111.5%, 37.2%, and 48.5%, respectively.

The ultra-broad band of the designed ALGs arises from the principle of linear superposition and ultra-broadband properties of the proposed phased unit cells, which are presented in notes 2, 3, 4, and 6 of the supplementary materials. These results highlight the potential of the designed ALGs for applications requiring broad frequency range operation.

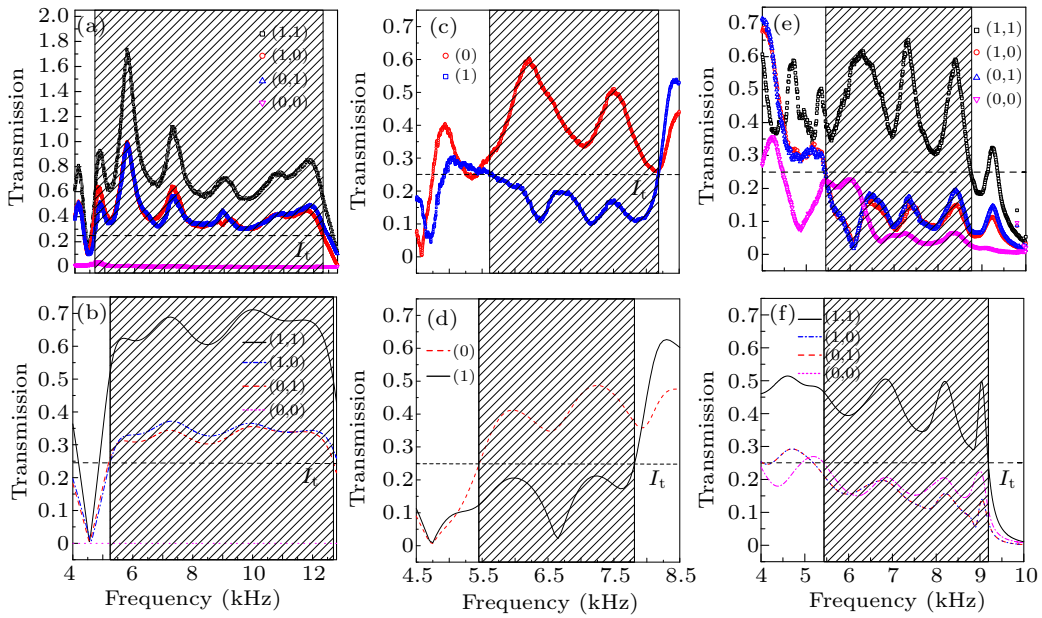


Fig. 6. Measured transmission spectra of the ALGs (a) OR, (c) NOT, and (e) AND, and the simulated ones of the ALGs (b) OR, (d) NOT, and (f) AND for different input states, respectively.

8. Conclusion

In conclusion, we have both numerically and experimentally demonstrated the ALGs with ultra-broad band performance, based on the circular waveguide structure with multiple ports and phased unit cells. The results show that the logic function OR has been well realized in a circular waveguide with an output port, two input ports and two phase unit cells II. Based on the phase manipulation of the phased unit cells II and the linear interference of sound, the measured fractional bandwidth of the ALG OR reaches about 111.5%, showing an ultra-broadband characteristic. Furthermore, by replacing one phased unit cell II in the ALG OR as the phased unit cell I, we have also realized the ALG NOT, and its measured fractional bandwidth reaches about 37.2%, which arises from the interference cancellation of sound at the output port O. In addition, by introducing the phased unit cells II and III, we have realized the logic function AND based on a circular waveguide with four ports, and the measured fractional bandwidth reaches about 48.5%. Meanwhile, the simulated transmission spectra of the ALGs OR, NOT, and AND have also been pre-

sented as comparison. The measured and simulated results are basically consisted with each other. The designed ALGs are characterized by ultra-broad band, simple structure and passive modulation, which have potential applications in the fields of acoustic information processing and logic operation, underwater communication, and so on.

Acknowledgement

Project supported by the National Natural Science Foundation of China (Grant No. 12174159).

References

[1] Zhang S C, Xue X Y, Chen C and Sun Z T 2019 *Int. J. Arg. Biol. Eng.* **12** 82
[2] Wang B, Du X X, Wang Y N and Mao H P 2024 *Int. J. Arg. Biol. Eng.* **17** 27
[3] Yang N, Xie L L, Pan C, Yuan M F, Tao Z H and Mao H P 2019 *J. Food Process. Eng.* **42** e12976
[4] Xu Y, Hassan M M, Ali S, Li H H, Ouyang Q and Chen Q S 2021 *J. Agric. Food Chem.* **69** 1667
[5] Chattopadhyay T and Roy J N 2013 *Opt. Commun.* **300** 119
[6] Xiu X M, Geng X, Wang S L, Cui C, Li Q Y, Ji Y Q and Dong L 2020 *Adv. Quantum Technol.* **2** 1900066
[7] Chinmoy M and Abhijit S 2023 *Opt. Quantum. Electron* **55** 906
[8] Gao X X, Chen B J, Shum K M, Zhang Q L, Ma Q, Cui W Y, Cui T J and Chan C H 2023 *Adv. Mater. Technol.* **8** 2201225
[9] Tian X Y, Li Q and Ren D H 2023 *Chin. Phys. B* **32** 057101
[10] Li L L, Luo J, Xia J, Zhou Y, Liu X X and Zhao G P 2023 *Chin. Phys. B* **32** 017506
[11] Azana J 2010 *IEEE Photon. J.* **2** 359
[12] Bie Y Q, Liao Z M, Zhang H Z, Li G R, Ye Y, Zhou Y B, Xu J, Qin Z X, Dai L and Yu D P 2011 *Adv. Mater.* **23** 649
[13] Wei H, Wang Z X, Tian X R, Käll M and Xu H X 2011 *Nat. Commun.* **2** 387
[14] Zhang Y X, Chen Y P and Chen X F 2011 *Appl. Phys. Lett.* **99** 161117
[15] Fu Y L, Hu X Y, Lu C C, Yue S, Yang H and Gong Q H 2012 *Nano Lett.* **12** 5784
[16] Abdulnabi S H and Abbas M N 2018 *J. Nanophotonics* **13** 016009
[17] Idres S, Habif J L and Hashemi H 2024 *Opt. Express* **32** 36063
[18] Liu Z Y, Zhang X X, Mao W Y, Zhu Y Y, Yang Z Y, Chan C T and Sheng P 2000 *Science* **289** 1734
[19] Lu M H, Zhang C, Feng L, Zhao J, Chen Y F, Mao Y W, Zi J, Zhu Y Y, Zhu S N and Ming N B 2007 *Nat. Mater.* **6** 744
[20] Torrent D and Sánchez-Dehesa J 2010 *Phys. Rev. Lett.* **105** 174301
[21] Wang P, Casadei F, Shan S, Weaver J C and Bertoldi K 2014 *Phys. Rev. Lett.* **113** 014301
[22] Lu J Y, Qiu C Y, Ke M Z and Liu Z Y 2016 *Phys. Rev. Lett.* **116** 093901
[23] Fang N, Xi D J, Xu J Y, Ambati M, Srituravanich W, Sun C and Zhang X 2006 *Nat. Mater.* **5** 452
[24] Li J, Fok L, Yin X B, Bartal G and Zhang X 2009 *Nat. Mater.* **8** 931
[25] Christensen J and de Abajo F J G 2012 *Phys. Rev. Lett.* **108** 124301
[26] Liang X Z and Li S J 2012 *Phys. Rev. Lett.* **108** 114301
[27] Quan L, Zhong X, Liu X Z, Gong X F and Johnson P A 2014 *Nat. Commun.* **5** 3188
[28] Li Y, Liang B, Gu X M, Zou X Y and Cheng J C 2013 *Sci. Rep.* **3** 2546
[29] Li Y, Shen C, Xie Y B, Li J F, Wang W Q, Cummer S A and Jing Y 2017 *Phys. Rev. Lett.* **119** 035503
[30] Assouar B, Liang B, Wu Y, Li Y, Cheng J C and Jing Y 2018 *Nat. Rev. Mater.* **3** 460
[31] Quan L, Sounas D L and Alù A 2019 *Phys. Rev. Lett.* **123** 064301
[32] Ma F Y, Wang C, Liu C R and Wu J H 2021 *J. Appl. Phys.* **129** 231103
[33] Wang Y, Zou H Y, Lu Y J, Gu S, Qian J, Xia J P, Ge Y, Sun H X, Yuan S Q and Liu X J 2023 *Prog. Electromagn. Res.* **177** 127
[34] Li F, Anzel P, Yang J, Kevrekidis P G and Daraio C 2014 *Nat. Commun.* **5** 5311
[35] Bringuier S, Swinteck N, Vasseur J O, Robillard J F, Runge K, Muralidharan K and Deymier P A 2011 *J. Acoust. Soc. Am.* **130** 1919
[36] Zhang T, Cheng Y, Guo J Z, Xu J Y and Liu X J 2015 *Appl. Phys. Lett.* **106** 113503
[37] Zhang T, Cheng Y, Yuan B G, Guo J Z and Liu X J 2016 *Appl. Phys. Lett.* **108** 183508
[38] Wang Y, Xia J P, Sun H X, Yuan S Q and Liu X J 2019 *Sci. Rep.* **9** 8355
[39] Lu Y J, Ge Y, Yuan S Q, Sun H X and Liu X J 2020 *J. Phys. D: Appl. Phys.* **53** 015301
[40] He H, Qiu C, Ye L, Cai X, Fan X, Ke M, Zhang F and Liu Z Y 2018 *Nature* **560** 61
[41] Ding Y J, Peng Y G, Zhu Y F, Fan X D, Yang J, Liang B, Zhu X F, Wan X G and Cheng J C 2019 *Phys. Rev. Lett.* **122** 014302
[42] Zhang X J, Lu M H and Chen Y F 2021 *Phys. Rev. Lett.* **126** 156401
[43] Xue H R, Yang Y H and Zhang B L 2022 *Nat. Rev. Mater.* **7** 974
[44] Xia J P, Jia D, Sun H X, Yuan S Q, Ge Y, Si Q R and Liu X J 2018 *Adv. Mater.* **30** 1805002
[45] Lu Y J, Wang Y, Ge Y, Yuan S Q, Jia D, Sun H X and Liu X J 2022 *Appl. Phys. Lett.* **121** 123506
[46] Ge Y, Shi B J, Jia D, Sun H Y, Xue H R, Yuan S Q and Zhang B L 2023 *Appl. Phys. Lett.* **123** 171703
[47] Li Y Y, Huang K Q, Gong M Y, Sun C H, Gao S L, Lai Y and Liu X Z 2024 *Results Phys.* **57** 107421
[48] Zuo C Y, Xia J P, Sun H X, Ge Y, Yuan S Q and Liu X J 2017 *Appl. Phys. Lett.* **111** 243501